Comparison of the electronic structures of four crystalline phases of $FePO_4$

Ping Tang, N. A. W. Holzwarth,* and Yaojun A. Du
Department of Physics, Wake Forest University, Winston-Salem, North Carolina 27109, USA
(Received 18 April 2007; revised manuscript received 9 October 2007; published 28 November 2007)

$LiFePO_4$ in the olivine structure is a promising cathode material for Li ion batteries. During normal battery operation, an olivine form of $FePO_4$ is produced. In addition to the olivine form, $FePO_4$ is known to form in a quartzlike structure, a high pressure $CrVO_4$-like structure, and a monoclinic structure. We report the results of a detailed density functional study of the electronic structures and total energies of these four crystalline structures of $FePO_4$. Partial density of states analysis of the four materials finds them all to be characterized by strong hybridization between the Fe and O contributions throughout their upper valence bands, consistent with recent x-ray spectroscopy studies of olivine $FePO_4$. Results obtained using the local density approximation for the exchange-correlation functional find the olivine structure to be more stable than the quartzlike structure by 0.1 eV, which is in good agreement with recent calorimetry experiments.

DOI: 10.1103/PhysRevB.76.174118 PACS number(s): 61.66.−f, 71.15.Mb, 71.15.Nc, 71.20.−b

I. INTRODUCTION

There has recently been a lot of interest in $FePO_4$ as the delithiated form of $LiFePO_4$ in connection with Li ion battery cathodes.[1] The mineral names "heterosite" and "olivine" have been used to describe this orthorhombic form of iron phosphate which has the space group symmetry *Pnma* (No. 62 in the *International Tables for Crystallography*[2]). Although the olivine structure has by far the best electrochemical properties, $FePO_4$ is known to crystallize in several different structures. The question of the stability of the olivine phase relative to the other forms is important for the possible adoption of $LiFePO_4$ in commercial batteries.

Yang *et al.*[3] showed that olivine $FePO_4$ irreversibly transforms to an electrochemically inactive quartzlike structure at ≈600 °C, suggesting that perhaps the olivine form might be metastable. In subsequent work, Song *et al.*[4] investigated the structural and electrochemical properties of several crystalline forms of $FePO_4$. In addition to the olivine and quartzlike structures, they studied a monoclinic form and also mentioned a high pressure form related to the $CrVO_4$ structure, more recently studied by Arroyo–de Dompablo *et al.*[5] In fact, very recently, Iyer *et al.*[6] carried out calorimetry measurements to show clear experimental evidence that the olivine structure is the more stable structure, suggesting that the irreversibility of the transformation to the quartz structure might be due to an activation barrier.

In order to study the factors which contribute to their stability, we undertook a series of first-principles simulations of the electronic structures of the four crystalline forms of $FePO_4$ mentioned above.[7] The outline of the paper is as follows. In Sec. II, we detail the computational methods used in this study. In Sec. III, we present the results of our lattice optimization (Sec. III A), densities of states (Sec. III B), and relative energies (Sec. III C). Discussions of the results are presented in Sec. IV and conclusions are presented in Sec. V.

II. CALCULATIONAL METHODS

All the calculations were performed within the framework of spin-dependent density functional theory (DFT)[8,9] using both the local density approximation (LDA)[10] and the generalized gradient approximation (GGA).[11] Symmetry breaking spin ordering within the unit cells and spin-orbit interactions were not included in the calculations. On the basis of the measured Neél temperature for the orthorhombic material,[12] we expect the error of that omission to be less than 0.01 eV per unit cell. During the course of this work, we used three different calculational methods and codes. The detailed analysis was carried out using our own PWPAW code,[13,14] which is based on the projector augmented wave (PAW) formalism developed by Blöchl.[15] More recently, we took advantage of the variable-cell optimization methods[16,17] that are available in the PWSCF code.[18] This code uses the ultrasoft pseudopotential (USPP) formalism of Vanderbilt,[19] which is conceptually and numerically very close to the PAW formalism. Since the treatment of spin dependence in the exchange-correlation functional was not initially available in our PWPAW code, we also used the WIEN2K code[20] based on the linear augmented wave (LAPW) method.[21] Fortunately, we found that by carefully adjusting the calculational parameters to ensure accuracy and convergence, we were able to obtain consistent results with all three methods.

Each of the computational methods uses specially designed atomic basis and potential functions. These functions are used to represent portions of the electronic wave functions in the vicinity of each atom. While they approximately span function space within the atomic spheres, they also must not be "overcomplete" and thus generate spurious "ghost" states.[22,23] We found that the default parameters of the WIEN2K code and the pseudopotentials on the web[18,19] are generally not able to represent the highly ionic materials in this study. The particular choice of parameters for the atomic basis and potential functions that we found to work well are listed in Table I. For the PAW and USPP formalisms, the r_c parameters indicate the "augmentation" sphere radii, representing spheres (that can slightly overlap) within which the atom-centered basis, projector, and pseudopotential functions are effective. For the LAPW calculation, the r_c parameters indicate muffin-tin radii, representing strictly nonoverlapping spheres within which the Kohn-Sham equations are analyzed with atom-centered basis functions. Also indicated in Table I are the basis functions used within each of the atomic

TABLE I. Atomic parameters used to generate atom-centered functions for the materials mentioned in this study, using the PAW (Ref. 13), USPP (Ref. 19), and LAPW (Ref. 20) codes. Essentially the same parameters were used with both the LDA (Ref. 10) and GGA (Ref. 11) exchange-correlation forms.

	r_c (bohr)	Atomic basis
		Li
PAW	1.61	$1s, 2s, 2p$
USPP	1.60	$1s, 2s, 2p$
LAPW	1.70	$1s, 2s, 2p$
		Fe
PAW	1.90	$3s, 4s, 3p, 4p, 3d, \epsilon d$
USPP	1.90	$3s, 4s, 3p, 4p, 3d, \epsilon d$
LAPW	1.95	$3s, \epsilon s, 3p, \epsilon p, \epsilon d$
		O
PAW	1.41	$2s, \epsilon s, 2p, \epsilon p$
USPP	1.40	$2s, \epsilon s, 2p, \epsilon p$
LAPW	1.28	$2s, \epsilon s, \epsilon p$
		P
PAW	1.51	$2s, 3s, 2p, 3p$
USPP	1.50	$3s, \epsilon s, 3p, \epsilon p, \epsilon d$
LAPW	1.38	$\epsilon s, 2p, \epsilon p$

spheres, with $1s, 2s, 2p, 3s, 3p, 3d, \ldots$ denoting the valence wave functions for the self-consistent neutral atom and $\epsilon s, \epsilon p, \epsilon d, \ldots$ indicating additional basis functions at energies ϵ used to improve the completeness of the representations. For these, the PAW and USPP parameters could be chosen to be nearly identical since they represent very similar formalisms generated with different computer codes, while the the LAPW parameters have somewhat different properties. While it is not the focus of the present work, Li is included in this table so that it can be used as a reference. Of the atoms included, P proved to be the most challenging due to the presence of ghost states within the energy range of interest. Fortunately, the ghost resonances could be shifted out of the important energy range by the careful selection of atomic basis functions.

In order to test the atomic parameters, we computed the total energy as a function of lattice parameter or bond length for several simple oxide materials. For this purpose, we calculated binding energy curves for Li_2O in the fluorite structure (Fig. 1) and FeO in the ferromagnetic NaCl structure (Fig. 2) and a hypothetical neutral tetrahedral PO_4 molecule (Fig. 3). (This PO_4 molecule, while convenient for testing purposes, is not known to exist in nature; natural phosphorus oxides are found in much more complicated structures.) For these three test materials, the three different computational methods give superposable binding energy curves, giving us confidence that the three methods can be used together to study the $FePO_4$ materials which are the focus of this study.

In addition to the atom-centered functions, the accuracy of the calculations are also controlled by the number of plane

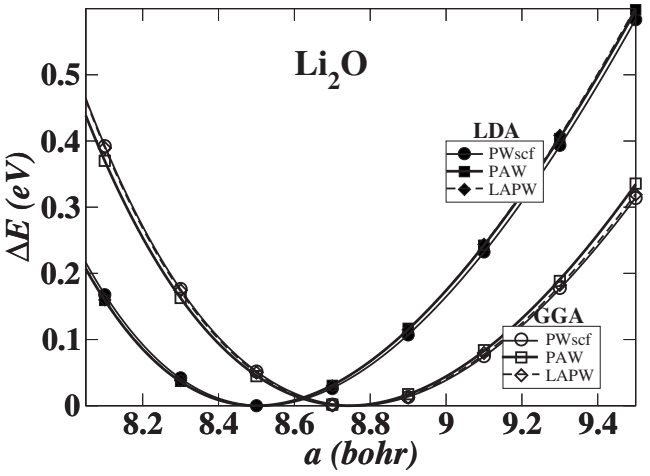

FIG. 1. Relative total energy versus the lattice constant of Li_2O in the fluorite structure obtained with the PWSCF (Ref. 18) PAW (Ref. 14) and LAPW (Ref. 20) computer codes. The set of curves indicated with the lighter lines and filled symbols with smaller equilibrium lattice constant was obtained with the LDA (Ref. 10) exchange-correlation form, while the other set of curves was obtained with the GGA (Ref. 11) exchange-correlation form.

waves included in the representation of the smooth portions of the wave functions. In this work, all plane wave coefficients were included in the wave function expansion with the cutoff criterion

$$|\mathbf{k}+\mathbf{G}|^2 \leq E_{\text{cut}}, \tag{1}$$

where $\mathbf{k}$ and $\mathbf{G}$ denote a Bloch wave vector and a reciprocal lattice vector, respectively. The values of E_{cut} were chosen to be 30 Ry for the LAPW code and 64 Ry for the PAW and PWSCF codes. The Brillouin zone integrals were performed using a Monkhorst-Pack[24] or similar scheme of uniform sampling within partitions of 0.15 bohr^{-1} or smaller on each side.

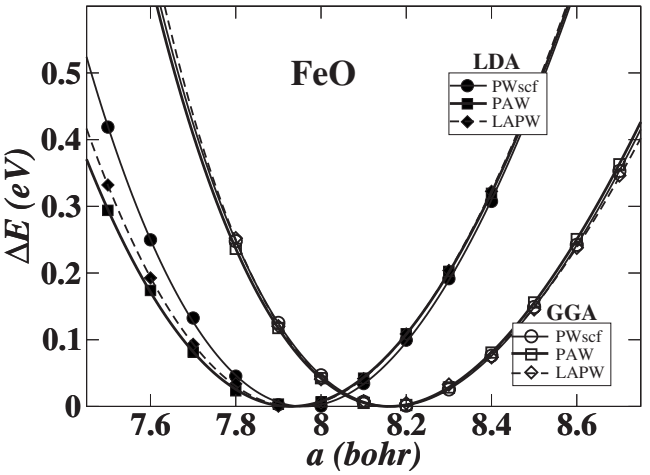

FIG. 2. Relative total energy versus lattice of FeO assuming a ferromagnetic NaCl structure, using the same conventions, as shown in Fig. 1.

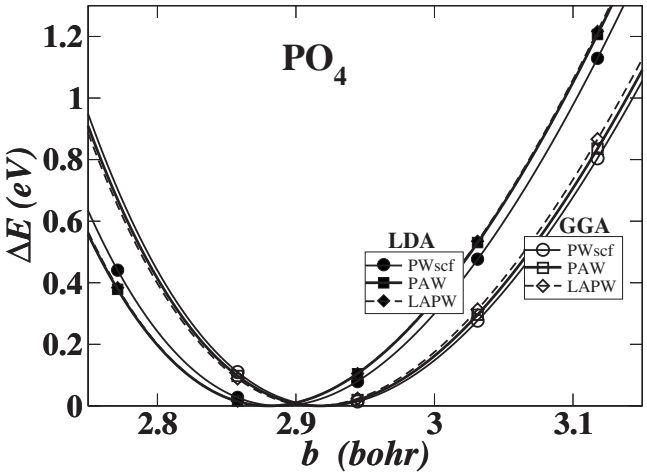

FIG. 3. Relative total energy versus bond length of a hypothetical neutral molecule of PO_4 assumed to have exact tetrahedral symmetry, using the same conventions, as shown in Fig. 1.

The partial densities of states were determined using a Gaussian shape function to replace the delta function,

$$N_\sigma^a(E) \equiv \frac{1}{\sqrt{\pi}\Delta} \sum_{n\mathbf{k}} f_{n\mathbf{k}\sigma}^a W_\mathbf{k} e^{-(E - E_{n\mathbf{k}\sigma})^2/\Delta^2}, \quad (2)$$

where $W_\mathbf{k}$ denotes the Brillioun zone weighting factor and the smearing parameter was chosen to be $\Delta = 0.1$ eV. The factor $f_{n\mathbf{k}\sigma}^a$ denotes the charge within a sphere about atom a with the radius taken to be the augmentation radius r_c^a given in Table I for each state of band index n, wave vector $\mathbf{k}$, and spin orientation σ.

For the PAW and LAPW schemes, structural optimization was carried out in two steps. For each choice of the lattice constants, the atomic positions were optimized within the symmetry constraints of their structures. The total energies were then fitted to a polynomial expansion of the energy in terms of the lattice parameters, in order to determine the optimized lattice constants. For the PWSCF scheme, structural optimization was determined by using variable-cell optimization methods.[16,17]

III. RESULTS

A. Crystal structures

Figures 4–7 show the four experimentally determined crystal structures of $FePO_4$ studied in the present work—the olivine, quartz, $CrVO_4$, and monoclinic forms, respectively. Evident from these figures is the fact that the Fe sites are coordinated by six nearest-neighbor O's in approximately octahedral geometry for the olivine and $CrVO_4$ structures. For the quartz structure, the Fe sites are coordinated by four nearest-neighbor O's in approximately tetrahedral geometry. By contrast, in the monoclinic structure, the Fe sites have lower symmetry and their coordination with nearest-neighbor O's is approximately 5.

In the chemical literature,[4] it is often noted that the octahedral coordination of Fe stabilizes its Fe^{+2} and Fe^{+3} charge states, while tetrahedral coordination stabilizes only its Fe^{+3} charge state. This trend is presumably related to different crystal field splittings of the Fe d states in octahedral and tetrahedral symmetries. Since the cathode reaction involves

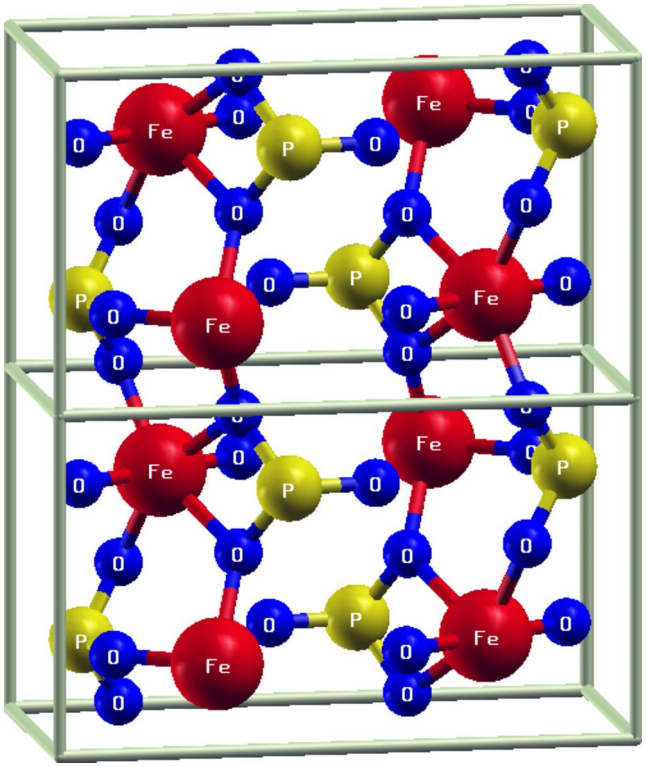

FIG. 4. (Color online) XCRYSDEN (Ref. 25) drawing of the olivine crystal structure. Fe, P, and O spheres are represented with spheres of decreasing size, with online colors red, yellow, and blue, respectively.

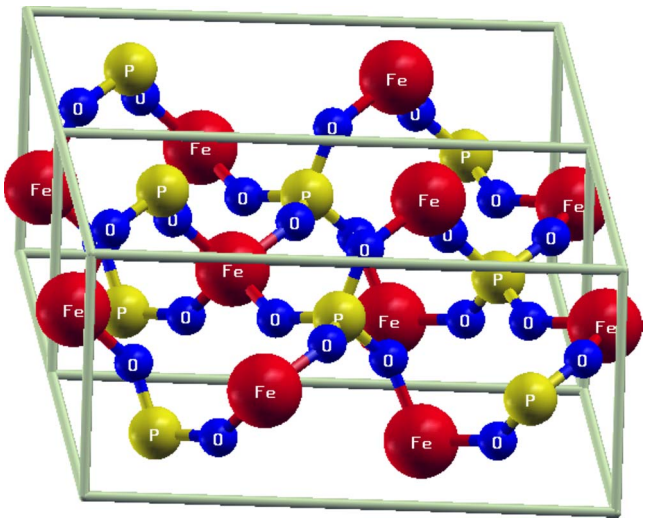

FIG. 5. (Color online) Quartz crystal structure, using the same convention, as in Fig. 4.

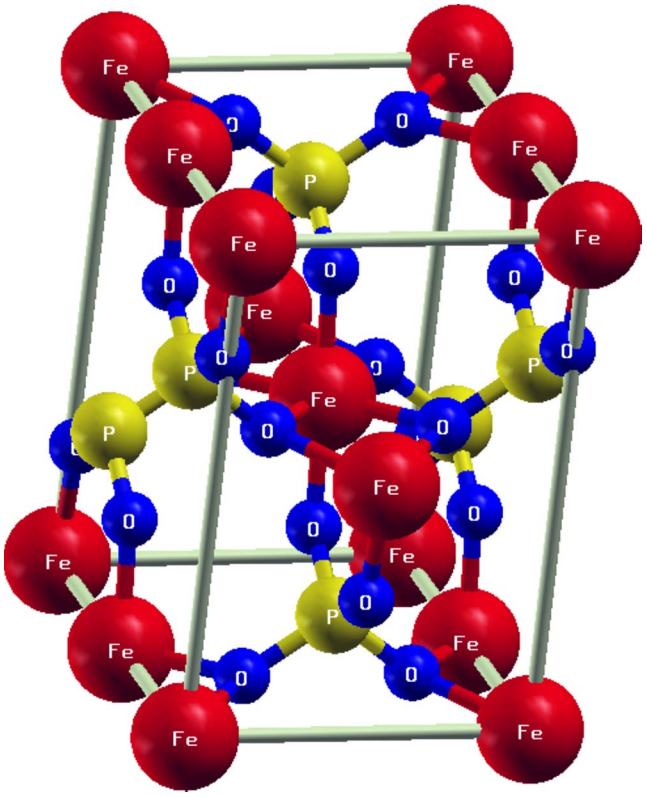

FIG. 6. (Color online) $CrVO_4$ crystal structure, using the same convention, as in Fig. 4.

transitions between the Fe^{+2} and Fe^{+3} charge states, it follows that the octahedrally coordinated structures—olivine and $CrVO_4$—would be expected to be more electrochemically active materials. However, recent experimental studies of the electrochemical properties of the $CrVO_4$ structured material[5] have shown that despite its favorable Fe coordination, the Li ion mobility in this material is too small to be technologically useful.

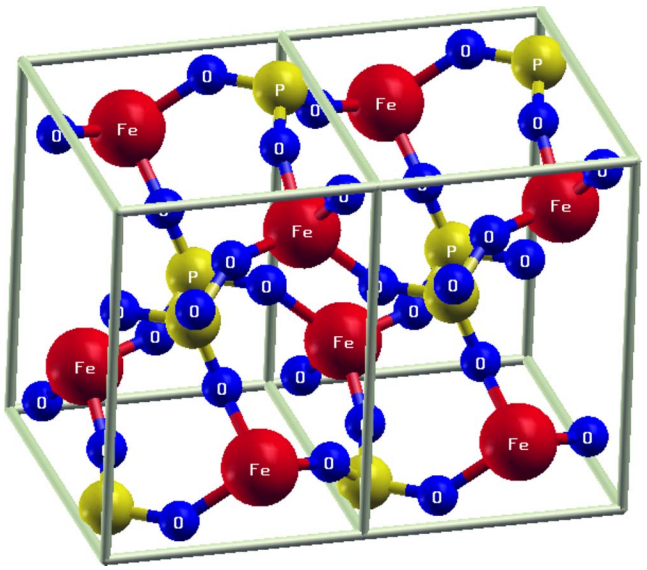

FIG. 7. (Color online) Monoclinic crystal structure, using the same convention, as in Fig. 4.

TABLE II. Lattice parameters for $FePO_4$. V denotes the volume per f.u. (Å^3), a, b, and c denote the lattice parameters (Å), and β (deg) is the nonorthogonal lattice angle for the monoclinic structure (optimized only with the PWSCF code).

	V	a	b	c	β
		Olivine ($Pnma$)			
LDA-LAPW	67.5	9.83	5.76	4.77	
LDA-PWSCF	68.1	9.85	5.77	4.79	
GGA-LAPW	74.5	10.04	6.01	4.94	
GGA-PAW	74.5	10.04	6.01	4.94	
GGA-PWSCF	74.0	10.03	5.99	4.93	
Expt.[a]	66.7	9.76	5.75	4.76	
		Quartz ($P3_121$)			
LDA-LAPW	79.9	4.99		11.12	
LDA-PWSCF	79.8	4.99		11.12	
GGA-LAPW	91.9	5.25		11.57	
GGA-PAW	91.9	5.25		11.57	
GGA-PWSCF	91.3	5.23		11.58	
Expt[b]	82.4	5.04		11.26	
		$CrVO_4$-type ($Cmcm$)			
LDA-LAPW	62.3	5.24	7.73	6.15	
LDA-PWSCF	62.8	5.23	7.76	6.19	
GGA-PWSCF	68.6	5.32	7.96	6.48	
Expt.[c]	64.3	5.23	7.78	6.33	
		Monoclinic ($P2_1/n$)			
LDA-LAPW	81.5	5.52	7.40	8.02	95.7
LDA-PWSCF	81.9	5.54	7.40	8.03	96.1
GGA-LAPW	91.3	5.47	8.03	8.36	95.7
GGA-PWSCF	88.4	5.60	7.68	8.27	96.5
Expt.[d]	82.1	5.48	7.48	8.05	95.7

[a]Reference 12.
[b]Reference 26.
[c]Reference 5.
[d]Reference 4.

Table II compares all of the calculated lattice constants with the experimental values for these structures. For the olivine, quartz, and $CrVO_4$ structures, we find that the lattice constants for the different calculational methods agree to better than ±0.03 Å. For the monoclinic structure, the agreement is somewhat less good: perhaps due to its more complicated geometry which includes a nonorthogonal lattice angle β and perhaps due to regions of low curvature in its potential energy surface. In general, the experimental results are closer to the LDA calculations, but the LDA calculations systematically underestimate the lattice constants, while the GGA calculations systematically overestimate the lattice constants. The optimized atomic coordinates in fractional units for the four crystal forms calculated with the PWSCF code for the LDA functional are listed in Table III. They agree with the experimental measurements within ±0.01 in

TABLE III. Fractional coordinates (x,y,z) for the inequivalent atoms in four crystalline forms of $FePO_4$, corresponding to the lattice parameters listed in Table II. Results calculated using the LDA-PWSCF scheme are compared to experimental diffraction measurements (rounded to three decimal digits).

		Calc.			Expt.		
Crystal	Atom	x	y	z	x	y	z
Olivine[a]	Fe	0.273	$\frac{1}{4}$	0.960	0.276	$\frac{1}{4}$	0.948
	P	0.095	$\frac{1}{4}$	0.406	0.094	$\frac{1}{4}$	0.395
	O_1	0.122	$\frac{1}{4}$	0.719	0.122	$\frac{1}{4}$	0.709
	O_2	0.443	$\frac{1}{4}$	0.151	0.439	$\frac{1}{4}$	0.160
	O_3	0.169	0.043	0.259	0.166	0.045	0.250
Quartz[b]	Fe	0.451	0.000	$\frac{1}{3}$	0.458	0.000	$\frac{1}{3}$
	P	0.448	0.000	$\frac{5}{6}$	0.458	0.000	$\frac{5}{6}$
	O_1	0.418	0.327	0.393	0.419	0.318	0.396
	O_2	0.403	0.271	0.873	0.413	0.264	0.875
$CrVO_4$[c]	Fe	0.000	0.000	0.000	0.000	0.000	0.000
	P	0.000	0.351	$\frac{1}{4}$	0.000	0.354	$\frac{1}{4}$
	O_1	0.000	0.241	0.046	0.000	0.246	0.050
	O_2	0.243	0.469	$\frac{1}{4}$	0.247	0.465	$\frac{1}{4}$
Mono[d]	Fe	0.390	0.810	0.060	0.388	0.806	0.060
	P	0.587	0.458	0.273	0.590	0.458	0.266
	O_1	0.493	0.649	0.236	0.481	0.640	0.228
	O_2	0.838	0.475	0.382	0.828	0.463	0.384
	O_3	0.619	0.357	0.111	0.641	0.358	0.116
	O_4	0.416	0.353	0.376	0.410	0.343	0.368

[a]Expt. from Ref. 12.
[b]Expt. from Ref. 26.
[c]Expt. from Ref. 5.
[d]Expt. from Ref. 4.

fractional units, except for a few of the O positions in the monoclinic structure. The ±0.01 error in fractional coordinates seems to be generally within the experimental uncertainty, as indicated by comparing coordinates for the olivine structure determined by x-ray[27] and neutron[12] diffraction. Similarly, the calculated and measured bond lengths listed in Table IV are in good agreement with experiment.

B. Densities of states

Results for the partial densities of states are presented in Fig. 8, calculated using Eq. (2), comparing the LDA and GGA results for the four crystal forms. The results show a systematic pattern of LDA bandwidths being larger and band gaps being smaller compared to the GGA results. However, the general form of the density of states is very similar among the four materials. The $CrVO_4$-type material is clearly metallic, while the other materials have band gaps at the Fermi level ranging from 0.1 (0.4) eV for the olivine structure to 0.8 (1.0) eV for the quartz structure using LDA (GGA) functionals. The relatively large calculated band gap for the quartz structure is consistent with its observed poor electrochemical activity.[4] By contrast, the metallic behavior of the $CrVO_4$-type material indicates that its electronic conductivity should be good; however, experimental results[5] suggest that poor ionic conductivity causes this material to have poor electrochemical activity.

The basic structure of the occupied densities of states for all of the materials in the range of $-10 \leq E \leq 0$ eV can be explained as follows. At the lowest order of approximation, the states correspond to the filled O $2p^6$ states and Fe ions in the configuration $3d_{\uparrow}^5 3d_{\downarrow}^0 4s^0$. The P ions formally lose all of their valence electrons. However, the partial densities of states show that the states at the low energy range have nontrivial P contributions which can be well described in terms of hybridization with the nearest-neighbor O ions to form P $3s$–O $2p\sigma$ states in the energy range of $-10 \leq E \leq -8$ eV and P $3p$–O $2p\sigma$ states in the energy range of $-8 \leq E \leq -6$ eV. For the quartz structure, this partitioning results in two separate groups of bands, while for the other structures, additional hybridizations complicate the form of the densities of states in this energy range. The use of the O $2p\sigma$ states in the formation of the P-O bonds leaves the O $2p\pi$ states, corresponding to four electrons per O, to form the upper portion of the valence band. The two majority spin electrons (O $2p\pi_{\uparrow}^2$) hybridize with the Fe $3d_{\uparrow}^5$ states and the two minority spin electrons (O $2p\pi_{\downarrow}^2$) form a narrower band in a

TABLE IV. Bond lengths (in Å) for four crystalline forms of $FePO_4$, corresponding to lattice and positional parameters listed in Tables II and III, calculated using the LDA-PWSCF scheme are compared to those deduced from experimental diffraction measurements.

Crystal	Bond	Calc.	Expt.
Olivine[a]	Fe-O_1	1.89	1.89
	Fe-O_2	1.90	1.89
	Fe-O_3	2.03	2.02
	Fe-O_3	2.13	2.14
	P-O_1	1.53	1.52
	P-O_2	1.57	1.53
	P-O_3	1.53	1.54
Quartz[b]	Fe-O_1	1.84	1.85
	Fe-O_2	1.86	1.87
	P-O_1	1.54	1.54
	P-O_2	1.54	1.53
$CrVO_4$[c]	Fe-O_1	1.89	1.94
	Fe-O_2	2.07	2.08
	P-O_1	1.53	1.52
	P-O_2	1.56	1.55
Mono[a]	Fe-O_1	1.89	1.87
	Fe-O_2	1.96	1.97
	Fe-O_2	2.14	2.24
	Fe-O_3	1.84	1.87
	Fe-O_4	1.85	1.81
	P-O_1	1.53	1.51
	P-O_2	1.57	1.54
	P-O_3	1.53	1.47
	P-O_4	1.53	1.60

[a]Expt. from Ref. 12.
[b]Expt. from Ref. 26.
[c]Expt. from Ref. 5.
[d]Expt. from Ref. 4.

similar energy range. The Fe $3d^0_\downarrow$ states form the lowest energy unoccupied states above the Fermi level. The formation of the O $2p\sigma$ bonds with P, leaving the O $2p\pi$ states to interact with the transition metal, is sometimes referenced as the "induction effect."[28] This same description of the valence state distribution generally fits all four of the crystal forms shown in Fig. 8 so that, in principle, all could be well described by closed-shell single determinant wave functions, except perhaps for the metallic contributions in the $CrVO_4$-type structure. Correspondingly, the calculated spin moments correspond to 5 μ_e per formula unit for all of the materials other than the $CrVO_4$ structure which has a slightly smaller spin moment.

The interesting fact that for olivine $FePO_4$ the upper valence band of the majority spin states can be described by well-hybridized Fe $3d_\uparrow$ and O $2p_\uparrow$ throughout the spectrum has been discussed in previous work[7,29] and is consistent with recent x-ray spectroscopy measurements.[30,31] From Fig. 8, it is apparent that the strong hybridization of Fe $3d_\uparrow$ and O $2p_\uparrow$ states throughout their valence band spectra is a feature of all of the $FePO_4$ materials.

Since the insightful paper by Sham and Schlüter,[32] it has been understood that an energy band gap calculated from the DFT eigenstates differs from the physical energy band gap by a self-energy correction. Since estimating this band gap correction is beyond the scope of the present work, any comparison to experimental band gaps is necessarily very qualitative. Previous calculations by other authors using DFT $+U$ techniques report much larger minimum band gaps that those of the present work. A minimum band gap of 1.9 eV was reported by Zhou *et al.*[33] for the olivine structure and (approximately) 1.4 eV was reported by Arroyo–de Dompablo *et al.*[5] for the $CrVO_4$ structure. Unfortunately, we know of no direct experimental measurements of the band gap of these materials with which the calculated results can be compared. Zhou *et al.*[33] cite a band gap of 4 eV for the related material $LiFePO_4$ on the basis of reflectance measurements which they find consistent with their DFT$+U$ calculations of that material. However, more recent work by Hunt *et al.*[30] find their inelastic x-ray scattering measurements to be more consistent with a much smaller band gap for $LiFePO_4$ as well as for $FePO_4$, as is consistent with the olivine density of states presented in Fig. 8.

C. Total energies

The results for the internal energy differences for $FePO_4$ materials relative to the olivine structure are summarized and compared with the experimental calorimetry measurements for the quartz and olivine crystals[6] in Table V. The table shows that the three independent computational methods give consistent results and that the range of the energy differences is quite small −0.2 (0.4) eV for LDA (GGA). The calculated LDA internal energy difference for the quartz structure relative to the olivine structure is close to the experimental result of 0.12 eV/$FePO_4$.[6]

For the LDA calculations, the ordering of the most stable to least stable structures is $CrVO_4$, monoclinic, olivine, and quartz. The LDA calculations also indicate that the monoclinic structure has nearly the same energy as the olivine structure, while the $CrVO_4$-type structure has an energy −0.1 eV/$FePO_4$ relative to that of the olivine structure. Thus, the LDA calculations suggest that the $CrVO_4$-type structure is the most stable of the four structures studied, which has yet to be verified by the experiment. The fact that the $CrVO_4$-type structure has been prepared under conditions of high pressure and temperature from the quartz structure[5,34–36] indicates that there is an activation barrier but does not provide information about the relative stability of the equilibrium structures.

By contrast, the GGA calculations give results for the relative stabilities essentially opposite to those of the LDA calculations, finding the quartz structure to have an energy −0.3 eV/$FePO_4$ relative to that of the olivine structure, in direct contradiction to the experimental result.[6] Since there is good agreement with available experiment, we expect that our LDA results provide the more reasonable analysis of four

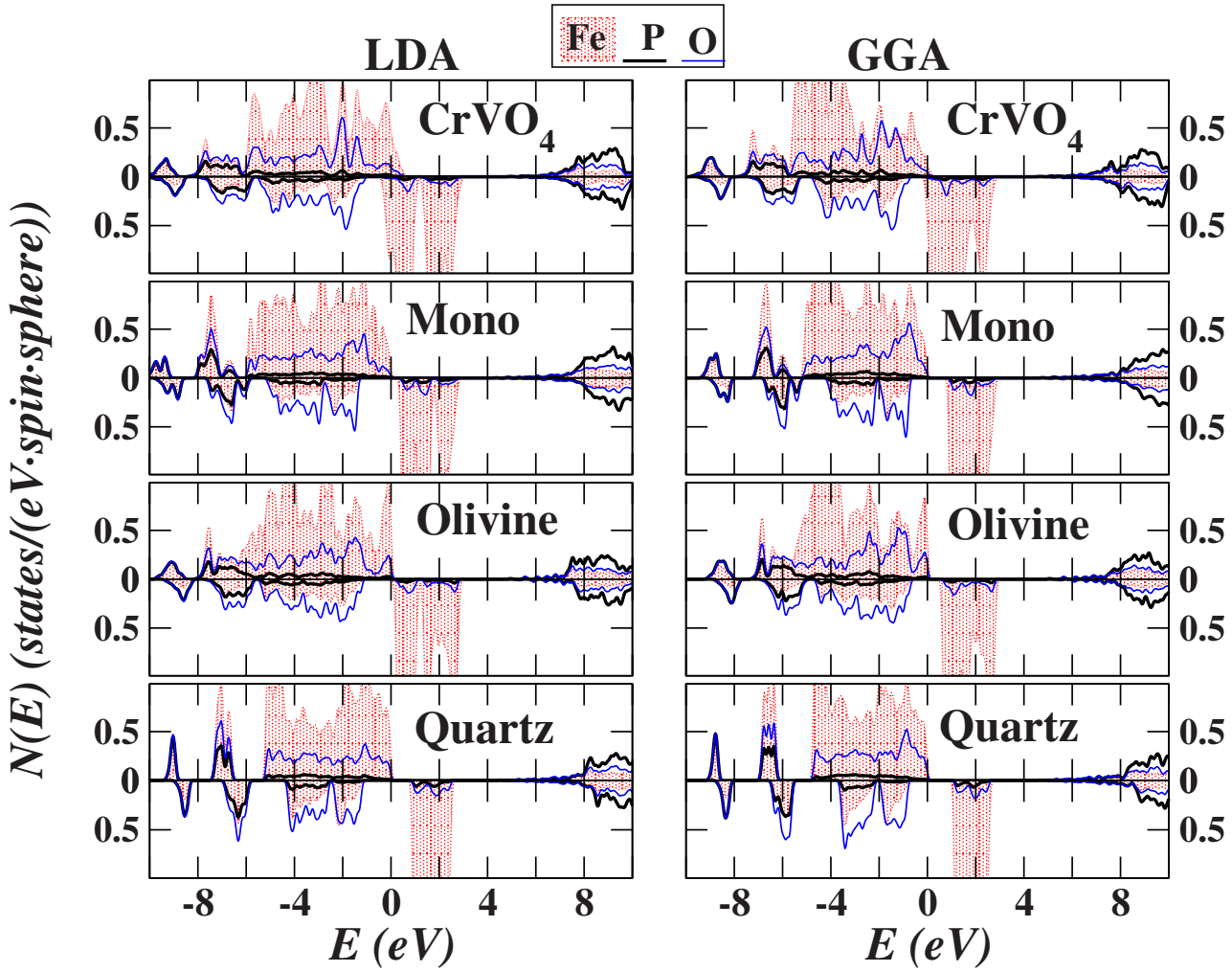

FIG. 8. (Color online) Partial densities of states for $FePO_4$ in the four different crystalline forms, comparing LDA (left) and GGA (right) results calculated using Eq. (2), plotting the majority and minority spin contributions upward and downward along the vertical axis, respectively. The zero of energy is taken to be the Fermi level.

TABLE V. Internal energies of the four crystalline forms of $FePO_4$ relative to the olivine structure (in units of $eV/FePO_4$).

Crystal	LDA	GGA	Expt.[a]
Olivine	0.00	0.00	0.00
Quartz	0.09 (LAPW)	−0.35 (LAPW)	0.12
	0.05 (PAW)	−0.27 (PAW)	
	0.09 (PWSCF)	−0.25 (PWSCF)	
$CrVO_4$-type	−0.10 (LAPW)		
	−0.11 (PAW)	0.07 (PAW)	
	−0.07 (PWSCF)	0.07 (PWSCF)	
Monoclinic	0.02 (LAPW)	−0.19 (LAPW)	
	−0.01 (PAW)	−0.16 (PAW)	
	−0.02 (PWSCF)	−0.17 (PWSCF)	

[a]Reference 6.

crystalline phases of $FePO_4$ including a plausible prediction of the correct relative stability.

IV. DISCUSSION

The fact that the LDA and GGA results for these calculations are significantly different from each other is not unprecedented. In our own work,[37] we have studied Li_3PO_4 in its β- and γ-crystal forms, finding that $E_\gamma - E_\beta = 0.03$ (0.01) $eV/FePO_4$ for the LDA (GGA) simulations, respectively. For this system, the LDA and GGA results differ by 0.02 eV, but they are both consistent in sign with each other and with experiment,[38] finding the β structure to be more stable than the γ phase.

There are several examples of material studies in the literature which document different structural and energetic results for LDA and GGA simulations. For example, in studies of phase transitions in silica, Hamann[39] found LDA andGGA calculations to give different relative energies for the α-quartz and stishovite forms of SiO_2. In that case, the GGA

results for the relative internal energies were in much better agreement with experiment. This work was later corroborated by Zupan *et al.*[40] who also studied the diamond and β-tin structures of Si and the bcc and fcc structures of metallic Fe, again finding the GGA results to be in closer agreement with experiment. Another example is a study of the group-III nitrides by Fuchs *et al.*[41] who found different trends in calculating structural properties and heats of formation with LDA and GGA functionals. These authors showed that the GGA calculations reproduce the crystal binding energies more consistently than the LDA calculations but significantly overestimate the binding energy of a N_2 molecule. Furche and Perdew[42] carried out a systematic comparison of several functionals including the LDA and GGA functionals used in the current work for a number of atomic and molecular systems. They conclude that for transition metal materials, "errors in the range of 10 kcal/mole [0.4 eV] per bond, sometimes more, have to be expected."

More recently, there has been considerable effort focused on reducing the errors of DFT simulations of transition metal materials. There are two main physical effects—strong correlation among the localized d electrons of the transition metal ions and the self-interaction error which can be quite large for the localized d electrons of the transition metal ions.

The standard definition of correlation is based on the deviation of the exact many-body wave function relative to a single Slater determinant. For transition metal materials with a partially filled d shell, these correlations could in principle be approximated by a sum over several Slater determinants to represent the correlation effects beyond average correlations embedded into the exchange-correlation functional. The so-called DFT+U scheme[43,44] has been developed as a first step toward including such effects. In the DFT+U approach, a Hubbard-like Coulomb repulsion at each Fe site is added to the Kohn-Sham Hamiltonian and its occupancy is treated in a self-consistent mean-field formalism. The repulsion parameter U can be either treated empirically or calculated self-consistently, while the occupation parameters are determined by suitable localized projector functions. Zhou *et al.*[45] successfully used this approach to model Li_xFePO_4 materials. They showed that by choosing U in a physically reasonable range, the expected charge-ordering behavior of Li_xFePO_4 could be successfully modeled. Their results showed that a majority of Fe sites had either Fe^{+3}(Fe III) or Fe^{+2}(Fe II) ions, which was consistent with the experimental evidence that Li_xFePO_4 tends to phase separate into $FePO_4$ and $LiFePO_4$ domains. The DFT+U approach was further able to make quantitative predictions of redox potentials of $FePO_4/LiFePO_4$ and other cathode materials.[46] More recently, this DFT+U approach has been applied to the very interesting problem of modeling electron transport in Li_xFePO_4, assuming a polaron mechanism of charge transfer between Fe^{+2} and Fe^{+3} sites.[47] Other research groups have also used the DFT+U approach to study these and similar materials.[33,48,49]

In summary, the most successful use of DFT+U techniques has come from the introduction of solutions which lower the symmetry of the system and thus approximate multideterminant effects. This approach is analogous to solutions of the Hubbard model itself,[50] where it has been shown that within a mean-field (Hartree-Fock) approach, a broken symmetry solution can sometimes approach the exact solution when the full symmetry solution fails. This was shown explicitly for the one-dimensional Hubbard model by Johansson and Berggren[51] where a broken symmetry antiferromagnetic solution was found to closely approximate the ground state energy, while the full symmetry Hartree-Fock solution yielded unphysical ground states at large values of the Coulomb repulsion parameter U. In a similar way, the MIT group[45–47] has been able to use the DFT+U technique to model transition metal compounds by stabilizing low symmetry configurations such as the Fe-ion sites of different charges within nonstoichiometric Li_xFePO_4. For materials which are expected to have uniform charge and/or spin on all of the transition metal sites, the DFT+U technique may have some value as a scheme to provide approximate self-interaction correction but may suffer the same inaccuracies of other uniform mean-field treatments. For this reason, we do not expect the DFT+U technique to be helpful for modeling $FePO_4$ in its various crystalline structures where for each crystal form, the Fe sites are geometrically and electronically equivalent. Furthermore, since we have argued that the $FePO_4$ materials are well represented by single determinant wave functions, there appears to be little reason to use techniques designed to treat highly correlated systems. The fact that experimental x-ray spectroscopy results[31,30] on olivine materials are in good agreement with the results of traditional DFT simulations provides experimental support for this argument.

The "self-interaction" error was identified in a 1981 paper by Perdew and Zunger,[52] who noticed that each occupied electron state $\Psi_{n\mathbf{k}\sigma}(\mathbf{r})$ repels itself in the self-consistent Coulomb interaction. In Hartree-Fock theory,[53] this unphysical self-repulsion is subtracted out explicitly, as shown in the following expression for the electronic Coulomb (E_C) and exchange (E_X) energies:

$$E_C + E_X = \frac{e^2}{2} \sum_{n\mathbf{k}\sigma} \sum_{n'\mathbf{k}'\sigma'} w_{n\mathbf{k}\sigma} w_{n'\mathbf{k}'\sigma'} \left[\frac{|\Psi_{n\mathbf{k}\sigma}(\mathbf{r})|^2 |\Psi_{n'\mathbf{k}'\sigma'}(\mathbf{r}')|^2}{|\mathbf{r}-\mathbf{r}'|} - \delta_{\sigma\sigma'} \frac{\Psi^*_{n\mathbf{k}\sigma}(\mathbf{r}) \Psi_{n'\mathbf{k}'\sigma'}(\mathbf{r}) \Psi_{n\mathbf{k}\sigma}(\mathbf{r}') \Psi^*_{n'\mathbf{k}'\sigma'}(\mathbf{r}')}{|\mathbf{r}-\mathbf{r}'|} \right]. \tag{3}$$

Here, the indices $n\mathbf{k}\sigma$ denote the band index, wave vector, and spin index, respectively, while $w_{n\mathbf{k}\sigma}$ denotes the Brillouin zone-weighted occupancy factor for the electronic state $\Psi_{n\mathbf{k}\sigma}(\mathbf{r})$. Both of these terms must be evaluated carefully for the infinite periodic system. The divergence of the electronic Coulomb energy E_C becomes well defined when combined with the corresponding nuclear interaction terms. The self-repulsion term which is subtracted from E_C in the exchange contribution E_X appears as an integrable singularity.[54,55] In

TABLE VI. Hartree-Fock exchange corrected LDA internal energies of the four crystalline forms of $FePO_4$ relative to the olivine structure (in units of eV/$FePO_4$) obtained using the WIEN2K code (Ref. 20) for various values of the strength parameter α.

α	Orbital	Olivine	Quartz	$CrVO_4$	Mono
0.00	Fe(d)	0.00	0.09	−0.10	0.02
0.35	Fe(d)	0.00	1.05	−0.08	0.16
1.00	Fe(d)	0.00	2.97	−0.08	0.43
1.00	Fe(d) and O(p)	0.00	3.22	0.39	0.87

the present work, E_C is represented as defined in Eq. (3), but since the exchange contribution is treated in the LDA or GGA formulation, the electron self-repulsion term is not canceled from the energy. Because of this singular behavior, the self-repulsion is numerically difficult to calculate directly and difficult to approximate consistently.

The are several suggestions in the literature of how to correct the self-interaction problem in an approximate way.[56–61] Since the error is large where the wave functions have the greatest amplitudes, most of these formulations are based on localized basis functions centered on the atomic sites. Although these methods have succeeded in making qualitative improvements to the modeling of the structures of several types of materials including those with transition metal and rare-earth components,[56–58,61] it is not clear that the accuracy of these methods is sufficient to tackle the delicate balance of crystal field and hybridization effects, and the relative importance of the Fe 3d and O 2p contributions, that stabilize the $FePO_4$ crystalline forms of the current study.

Nevertheless, in order to get an estimate of the self-interaction error, we have taken advantage of a muffin-tin-based formulation recently developed in the WIEN2K code.[20,62,63] In this formulation, the spherical average of the l-projected density within a muffin sphere is used to define the square of a radial function $\chi_l(r)$ from which the Slater integral F^k [defined in Eq. (7) of Ref. 63] is calculated. The Hartree-Fock exchange contributions within the muffin-tin spheres are then calculated from summations of the Slater integrals F^k times the appropriate angular weight factors determined from the occupied states. The correction to the energy is generally given in the form

$$\Delta E = \alpha(E_x^{HF} - E_x^{DFT}), \tag{4}$$

where E_x^{HF} and E_x^{DFT} denote the sum of the muffin-tin contributions of the exchange energy calculated using the Hartree-Fock and density functional formulations, respectively. The strength factor α is an adjustable parameter which we took to be 1 or 0.35, representing full Fock exchange or a popular choice[63] for hybrid Fock exchange, respectively. Table VI lists the results of our calculations which were obtained using the LDA-PWSCF geometries and the LDA functional, comparing results for various values of α including the corresponding α=0 values reproduced from Table V. Results obtained by including only Fe(d) contributions show that the relative energy of the $CrVO_4$ structure is only slightly changed, while the relative energies of the monoclinic and quartz structures are raised by a significant amount for both choices of α. This trend shows that the correction is very sensitive to the extent of the Fe(d) wave functions, correlating with the number of O neighbors—olivine and $CrVO_4$ structures having six neighbors and the smallest correction and the quartz structure having four neighbors and the largest correction. Since the O 2p states are almost as spatially localized as are the Fe 3d states, it is sensible to consider both Fe(d) and O(p) contributions in these calculations; however, since the muffin-tin radius of O is quite small, the approximation works less well and the calculations converge very slowly. The corresponding results listed in Table VI suggest that the O(p) states do have a substantial contribution to the self-interaction correction. These results offer a glimpse into some of the issues of the self-interaction correction, but obviously more work must be done for quantitative evaluation.

V. SUMMARY

In this work, we compare the electronic structures of four crystalline phases of $FePO_4$ using spin-dependent density functional theory with both LDA and GGA exchange-correlation functionals. By careful use of three independent computational formalisms and codes, the numerical accuracy is well controlled.

The partial densities of states of the four crystals differ in bandwidths and band gaps, but all have similar features which can be described by the following simple picture. The lowest states are due to σ bonds between the O 2p and P 3s and 3p states which form the strong P-O bonds. This so-called "induction" effect is responsible for there being only four 2p electrons for each O^{-2} ion to hybridize with the Fe 3d states. In fact, because of the strong spin coupling effects in Fe, the upper valence band is formed from a well-hybridized configuration of O $2p_\uparrow^2$ and Fe $3d_\uparrow^5$ for the majority spin, leaving the O $2p_\downarrow^2$ states to form a narrower band at a similar energy for the minority spin contribution. The minority spin Fe $3d_\downarrow^0$ states form a relatively narrow band above the Fermi level. This analysis provides evidence that these materials are well approximated as closed-shell systems and well described by single Slater determinant wave functions. The density of states spectrum for the olivine structure is consistent with recent x-ray spectroscopy measurements.[30,31]

Results for the lattice parameters are slightly underestimated by the LDA functional and overestimated by the GGA functional results, while the fractional atomic positions and bond lengths are generally in excellent agreement with experiment.

The relative energies of the four crystalline phases are very small—with internal energy differences of less than 0.2 (0.4) eV/$FePO_4$ for the LDA (GGA) results. The LDA functional results find the quartz structure to have a higher energy than that of the olivine structure by 0.1 eV, which is consistent with experiment,[6] and predict the $CrVO_4$ structure to be

the most stable. Further work examining the effects of the self-interaction error on these materials is suggested.

ACKNOWLEDGMENTS

This work was supported by NSF Grants Nos. NSF DMR-0405456 and DMR-0427055 and benefited from discussions with Yonas Abraham, Xiao Xu, Ronald Noftle, Abdessadek Lachgar, and G. E. Matthews at Wake Forest University. Computations were performed on the DEAC cluster at Wake Forest University which benefited from IBM SUR grants.

*natalie@wfu.edu; URL: www.wfu.edu/~natalie

[1] A. K. Padhi, K. S. Nanjundaswamy, and J. B. Goodenough, J. Electrochem. Soc. **144**, 1188 (1997).
[2] *International Tables for Crystallography, Volume A: Space-Group Symmetry*, 5th ed., edited by T. Hahn (Kluwer, Dordrecht, 2002).
[3] S. Yang, Y. Song, P. Y. Zavalij, and M. S. Whittingham, Electrochem. Commun. **4**, 239 (2002).
[4] Y. Song, P. Y. Zavalij, M. Suzuki, and M. S. Whittingham, Inorg. Chem. **41**, 5778 (2002).
[5] M. E. Arroyo–de Dompablo, J. M. Gallardo-Amores, and U. Amador, Electrochem. Solid-State Lett. **8**, A564 (2005).
[6] R. G. Iyer, C. Delacourt, C. Masquelier, J.-M. Tarascon, and A. Navrotsky, Electrochem. Solid-State Lett. **9**, A46 (2006).
[7] P. Tang, Ph.D. thesis, Wake Forest University, 2006, containing details of the work reported here.
[8] P. Hohenberg and W. Kohn, Phys. Rev. **136**, B864 (1964).
[9] W. Kohn and L. J. Sham, Phys. Rev. **140**, A1133 (1965).
[10] J. P. Perdew and Y. Wang, Phys. Rev. B **45**, 13244 (1992).
[11] J. P. Perdew, K. Burke, and M. Ernzerhof, Phys. Rev. Lett. **77**, 3865 (1996); Phys. Rev. Lett. **78**, 1396 (1997).
[12] G. Rousse, J. Rodriguez-Carvajal, S. Patoux, and C. Masquelier, Chem. Mater. **15**, 4082 (2003).
[13] N. A. W. Holzwarth, A. R. Tackett, and G. E. Matthews, Comput. Phys. Commun. **135**, 329 (2001); available from http://pwpaw.wfu.edu
[14] A. R. Tackett, N. A. W. Holzwarth, and G. E. Matthews, Comput. Phys. Commun. **135**, 348 (2001); available from http://pwpaw.wfu.edu
[15] P. E. Blöchl, Phys. Rev. B **50**, 17953 (1994).
[16] M. Parrinello and A. Rahman, Phys. Rev. Lett. **45**, 1196 (1980).
[17] R. M. Wentzcovitch, Phys. Rev. B **44**, 2358 (1991).
[18] S. Baroni, A. Dal Corso, S. de Gironcoli, P. Giannozzi, C. Cavazzoni, G. Ballabio, S. Scandolo, G. Chiarotti, P. Focher, A. Pasquarello, K. Laasonen, A. Trave, R. Car, N. Marzari, and A. Kokalj, available from http://www.pwscf.org/
[19] D. Vanderbilt, Phys. Rev. B **41**, 7892 (1990); USPP code is available from http://www.physics.rutgers.edu/~dhv/uspp/
[20] P. Blaha, K. Schwarz, G. Madsen, D. Kvasnicka, and J. Luitz, *WIEN2k, An Augmented Plane Wave + Local Orbitals Program for Calculating Crystal Properties* (Karlheinz Schwarz, Techn. Universität Wien, Vienna, 2001); http://www.wien2k.at
[21] O. K. Andersen, Phys. Rev. B **12**, 3060 (1975).
[22] X. Gonze, P. Käckell, and M. Scheffler, Phys. Rev. B **41**, 12264 (1990).
[23] X. Gonze, R. Stumpf, and M. Scheffler, Phys. Rev. B **44**, 8503 (1991).
[24] H. J. Monkhorst and J. D. Pack, Phys. Rev. B **13**, 5188 (1976).
[25] A. Kokalj, J. Mol. Graphics Modell. **17**, 176 (1999).
[26] H. N. Ng and C. Calvo, Can. J. Chem. **53**, 2064 (1975).
[27] A. S. Andersson, B. Kalska, L. Häggström, and J. O. Thomas, Solid State Ionics **130**, 41 (2000).
[28] A. K. Padhi, K. S. Nanjundaswamy, C. Masquelier, S. Okada, and J. B. Goodenough, J. Electrochem. Soc. **144**, 1609 (1997).
[29] P. Tang and N. A. W. Holzwarth, Phys. Rev. B **68**, 165107 (2003).
[30] A. Hunt, W. Y. Ching, Y. M. Chiang, and A. Moewes, Phys. Rev. B **73**, 205120 (2006).
[31] A. Augustsson, G. V. Zhuang, S. M. Butorin, J. M. Osorio-Guillén, C. L. Dong, R. Ahuja, C. L. Chang, P. N. Ross, J. Nordgren, and J. H. Guo, J. Chem. Phys. **123**, 184717 (2005).
[32] L. J. Sham and M. Schlüter, Phys. Rev. B **32**, 3883 (1985).
[33] F. Zhou, K. Kang, T. Maxisch, G. Ceder, and D. Morgan, Solid State Commun. **132**, 181 (2004).
[34] N. Kinomura, M. Shimada, M. Koizumi, and S. Kume, Mater. Res. Bull. **11**, 457 (1976).
[35] M. P. Pasternak, G. K. Rozenberg, A. P. Milner, M. Amanowicz, T. Zhou, U. Schwarz, K. Syassen, R. D. Taylor, M. Hanfland, and K. Brister, Phys. Rev. Lett. **79**, 4409 (1997).
[36] C. Murli, S. M. Sharma, S. K. Kulshreshtha, and S. K. Sikka, Pramana, J. Phys. **49**, 285 (1998).
[37] Y. A. Du and N. A. W. Holzwarth, Phys. Rev. B **76**, 174302 (2007).
[38] R. M. Rojas, J. L. M. de Vidales, A. Delgado, and J. V. Sinisterra, J. Solid State Chem. **106**, 237 (1993).
[39] D. R. Hamann, Phys. Rev. Lett. **76**, 660 (1996).
[40] A. Zupan, P. Blaha, K. Schwarz, and J. P. Perdew, Phys. Rev. B **58**, 11266 (1998).
[41] M. Fuchs, J. L. F. Da Silva, C. Stampfl, J. Neugebauer, and M. Scheffler, Phys. Rev. B **65**, 245212 (2002).
[42] F. Furche and J. P. Perdew, J. Chem. Phys. **124**, 044103 (2006).
[43] V. I. Anisimov and A. I. Lichtenstein, in *Strong Coulomb Correlations in Electronic Structure Calculations: Beyond The Local Density Approximation*, edited by V. I. Anisimov (Gordon and Breach, New York, 2000), Chap. 2, pp. 97–165.
[44] V. I. Anisimov, F. Aryasetiawan, and A. I. Lichtenstein, J. Phys.: Condens. Matter **9**, 767 (1997).
[45] F. Zhou, C. A. Marianetti, M. Cococcioni, D. Morgan, and G. Ceder, Phys. Rev. B **69**, 201101(R) (2004).
[46] F. Zhou, M. Cococcioni, C. A. Marianetti, D. Morgan, and G. Ceder, Phys. Rev. B **70**, 235121 (2004).
[47] T. Maxisch, F. Zhou, and G. Ceder, Phys. Rev. B **73**, 104301 (2006).
[48] O. Le Bacq, A. Pasturel, and O. Bengone, Phys. Rev. B **69**, 245107 (2004).
[49] M. E. Arroyo–de Dompablo, U. Amador, and F. Garcia-Alvarado, J. Electrochem. Soc. **153**, A673 (2006).
[50] J. Hubbard, Proc. R. Soc. London, Ser. A **276**, 238 (1963).
[51] B. Johansson and K.-F. Berggren, Phys. Rev. **181**, 855 (1969).

[52] J. P. Perdew and A. Zunger, Phys. Rev. B **23**, 5048 (1981).
[53] D. R. Hartree, *The Calculation of Atomic Structures* (Wiley, New York, 1957), pp. 85–86.
[54] F. Gygi and A. Baldereschi, Phys. Rev. B **34**, 4405 (1986).
[55] C. Kittel, *Quantum Theory of Solids (Second Revised Printing)* (Wiley, New York, 1987), Chap. 5.
[56] A. Svane, Phys. Rev. Lett. **72**, 1248 (1994).
[57] D. Vogel, P. Krüger, and J. Pollmann, Phys. Rev. B **54**, 5495 (1996).
[58] T. Fujiwara, M. Arai, and Y. Ishii, in *Strong Coulomb Correlations in Electronic Structure Calculations: Beyond The Local Density Approximation*, edited by V. I. Anisimov (Gordon and Breach, New York, 2000), Chap. 3, pp. 167–201.
[59] O. A. Vydrov, G. E. Scuseria, J. P. Perdew, A. Ruzsinszky, and G. I. Csonka, J. Chem. Phys. **124**, 094108 (2006).
[60] B. Baumeier, P. Krüger, and J. Pollmann, Phys. Rev. B **73**, 195205 (2006).
[61] B. Baumeier, P. Krüger, and J. Pollmann, Phys. Rev. B **75**, 045323 (2007).
[62] P. Novák, J. Kuneš, L. Chaput, and W. E. Pickett, Phys. Status Solidi B **243**, 563 (2006).
[63] F. Tran, P. Blaha, K. Schwarz, and P. Novák, Phys. Rev. B **74**, 155108 (2006).